Modeling the Large-Strain Constitutive Behavior of Polycarbonate under Isothermal and Anisothermal Conditions

J. Sweeney, P. Caton-Rose, P. D. Coates

IRC in Polymer Science and Technology, School of Engineering, Design and Technology, University of Bradford, Bradford BD7 1DP, United Kingdom

Received 8 March 2004; accepted 4 October 2004
DOI 10.1002/app.21681
Published online in Wiley InterScience (www.interscience.wiley.com).

ABSTRACT: The tensile behavior of polycarbonate was studied at large strains below the glass-transition temperature. Experiments were carried out at a series of constant temperatures and also under conditions of falling temperatures. The specimens necked with a natural draw ratio of approximately 2, and the study was mainly focused on the necked material. Isothermal experiments revealed an elastic mechanism that initiated beyond the natural draw ratio. A model consisting of an Eyring process and two Gaussian elastic mechanisms was found to be applicable to both the isothermal and anisothermal stress-relaxation and stress–strain results. The same model also produced reasonable estimates of the stresses generated during the necking process. In addition, a simple relationship between the isothermal and anisothermal stress relaxation was demonstrated.
 J Appl Polym Sci 96: 2105–2116, 2005

Key words: mechanical properties; necking; orientation; polycarbonates; viscoelastic properties

INTRODUCTION

There are many key polymer processes in which large stretches are imposed in the solid phase. Generally, they are complex and include steps under both solid and melt conditions. Increasingly, researchers are applying mathematical modeling to specify the process conditions associated with desirable product dimensions or properties. At the heart of any such model is a constitutive equation that must describe the material behavior at an appropriate level; its nature will be governed in part by the characteristics of the material and in part by what aspects of the product are to be predicted.

Solid-phase deformation processes normally produce oriented polymers with enhanced mechanical properties. There is clearly interest in the level of orientation and the associated improvements in the elastic modulus and other characteristics of the final cooled product. Typically, a process will involve stretching at a high temperature and then cooling at an approximately constant strain. For predicting the dimensions of a stretched product, modeling under the assumption of isothermal conditions can prove adequate.[1] However, the prediction of the mechanical properties of the final product requires a more sophisticated approach. A possible strategy is to create an integrated model that includes solid-phase processing, subsequent cooling, and finally mechanical testing that defines the properties of interest. At the heart of such a model is the requirement for a material constitutive equation that functions under conditions of varying temperatures. The development of such an anisothermal constitutive equation was the motivation for this study.

Polycarbonate, stretched uniaxially at elevated temperatures below the glass transition, is the focus of our studies. The material is nonlinear and viscoelastic and includes necking and yieldlike effects. We have studied the stress-relaxation and stress–strain behaviors both isothermally and under conditions of controlled cooling. On the basis of the observations, we have constructed a constitutive equation, involving an Eyring process and an elastic network, that models both the isothermal and anisothermal behaviors over a wide range of strain rates.

BACKGROUND

Anisothermal mechanical behavior

There have been a few studies of the mechanical behavior of polymers at various temperatures. Lai and Findley[2] studied the nonlinear creep behavior of polyurethane under conditions of continuously varying temperatures. They adopted a mathematical approach to model their results, and they used superposition

Correspondence to: J. Sweeney (j.sweeney@bradford.ac.uk).

integral techniques. More recently, Buckley[3] made a theoretical study of the linear, viscoelastic case with particular reference to the form of the temperature dependence. He produced a useful intuitive model of a parallel arrangement of spring-switch elements, each of which is elastic but only becomes active at a critical temperature. Upon cooling, the modulus of the material increases as more springs become active, but the effect of the increase in the modulus does not apply to strains imposed previously at a higher temperature. Drozdov[4] devised a model of adaptive links for the anisothermal case. This was also confined to linear viscoelastic materials, but the basic approach was considered to be extendable to the nonlinear case.

Studies of polycarbonate

As is well known,[5] the tensile drawing behavior of polycarbonate depends markedly on whether the temperature is above or below the glass transition. Above the glass transition, it extends homogeneously, whereas at lower temperatures, necking occurs. For this reason, processing in practice is normally done above the glass-transition temperature. However, its behavior at lower temperatures is of particular interest, and both the necking[6,7] and constitutive behaviors have been studied.[7–10] The material exhibits yieldlike behavior, with the yield stress dependent on the strain rate. A physically based mechanism that incorporates these effects is a desirable feature of a constitutive model. Thus, many workers[11–13] have made use of the Eyring process[14] for this purpose. An alternative mechanism is that of Argon,[15] and it has been incorporated into constitutive models developed by Boyce and coworkers[7,8,16] and by Wu and van der Giessen.[17] The latter researchers developed fully three-dimensional constitutive equations that combine the yield mechanism with large-deformation elastic models of the polymer network. Such models, when implemented within finite element analyses, have the potential to predict general deformations, including the evolution of necks in tensile specimens.[7,8]

Proposed approach

We are interested in the general principles of time-dependent and yieldlike behavior and how such principles can be extended from the isothermal case to the anisothermal case. This study at this stage is confined to one-dimensional behavior. We make use of the Eyring model together with a rubber elastic network; the combination of large elastic deformation and plasticity has a number of precedents.[7,8,16,17] However, the one-dimensional nature of our study precludes the use of sophisticated elastic networks, which require multiaxial experiments for the full definition of the material parameters. We have used an approach similar to that first used by Haward and Thackray,[18] combining an Eyring mechanism with a Gaussian network, to produce a constitutive model that can be naturally generalized to anisothermal conditions. We also show that, in the case of stress relaxation, a simple rule can be used to derive the anisothermal curve obtained during cooling from isothermal curves covering the relevant temperature range.

EXPERIMENTAL

The material was Bayer (Leverkusen, Germany) Macrolon polycarbonate, and it was obtained in a commercial sheet form 3 mm thick. It had a weight-average molecular weight of 35,000–37,000 and a glass-transition temperature of 148°C.[19] Plane tensile specimens, with a gauge length of 20 mm and a cross section of 10×3 mm^2, were cut from the sheet. Our area of detailed study was a set of experiments at constant temperatures of 110, 120, and 130°C and at temperatures varying within this range. Other tests at higher temperatures, some above the glass transition, were performed for comparison. For all the tests reported here, we used an Instron testing machine in conjunction with an environmental chamber. The specimens were illuminated and viewed through a window in the environmental chamber, and this enabled digital images to be captured for the purpose of strain measurements. For this purpose, square meshes with a cell size of 2 mm were silk-screen-printed onto the specimen surfaces. Images were captured at intervals of 2 s.

All the experiments were begun by the rapid (1.67 mm s^{-1}) stretching of the specimens at a constant crosshead speed. The deformation ceased to be uniform at a small strain, at which point shear banding started, usually at one end of the gauge length. The band, initially at 45° to the specimen axis, rapidly evolved into an approximately symmetric neck. The neck propagated until the whole gauge length consisted of necked material, in an approximately uniform state of strain. This process was complete after a specimen extension of 20 mm, when the extension ratio in the gauge length was on average 2.08. A further extension of the specimen of 8 mm was possible before fracture, corresponding to an extension ratio of 2.15 on average. This gave us the opportunity for experiments on uniformly deformed material within a narrow range of strain. In addition, we could capture by video imaging the nonuniform strain field during neck development and derive strains with a development of the method of Haynes and Coates.[20] In Figure 1, we show a specimen in its undeformed, necking, and fully necked states.

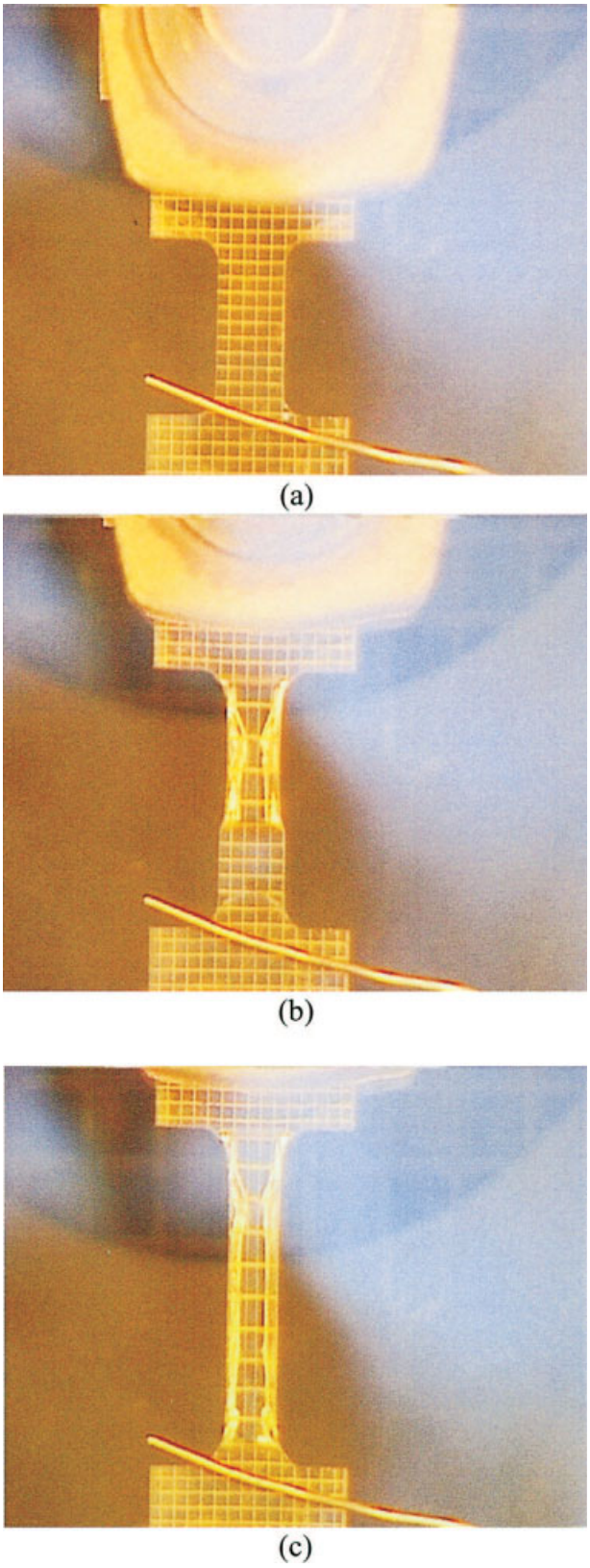

Figure 1 Tensile specimen at 130° in (a) undeformed, (b) partly necked, and (c) fully necked states.

Isothermal experiments

We examined the development of the temperature field within the specimen by placing a thermocouple into a 1-mm-diameter axial hole in the gauge length. A 15-min period was found to be sufficient for the attainment of steady conditions. Once steady thermal conditions were attained, the specimen was strained rapidly to the approximately uniform state as described previously. After this stage, there were two possibilities: either the testing machine was stopped for stress relaxation or deformation was continued at a different rate for a stress–strain experiment. We performed both kinds of experiments at 110, 120, and 130°C.

Stress relaxations were at extension ratios of 2.08 or 2.15. The lower strain was the smallest possible that was consistent with an essentially uniform state after necking, whereas the larger strain was the highest attainable before fracture. Given that the motivation of our study was the modeling of the stresses and strains in a stretched, cooling product, this range adequately covered the expected changes in strain.

We made a detailed study of the stress–strain behavior at 130°C. After the initial fast stretching to a uniform state of tensile strain at an extension ratio (λ) of 2.08 (extension = 20 mm), further stretching was performed at speeds varying from 6×10^{-4} to 2×10^{-2} mm s^{-1}. Strain rates for the specimen gauge lengths were obtained by image capture, and we found that they were essentially constant throughout the experiments (despite deformation outside the gauge area of the specimens) in the range of 5.0×10^{-6} to 1.7×10^{-4} s^{-1}.

Cooling experiments

During the isothermal experiments, steady temperature conditions were commonly achieved by the air temperature being kept constant for sufficient time, after which it was is assumed that the specimen and the associated loading members were no longer subject to thermal expansion. For the anisothermal experiments, steady temperature conditions were not achieved, and we had to make allowances for thermal deformation, most of which occurred in the metal loading train components.

To perform an experiment under conditions of cooling, we followed the following sequence of events. From room temperature, the specimen and apparatus were heated at a constant rate up to a set temperature, which was then kept constant. During this period, free thermal expansion was allowed. At the end of the period, steady conditions had been reached, and the specimen was stretched, through a necking state to an approximately uniform state of strain, as described previously. There followed a regimen of cooling at a

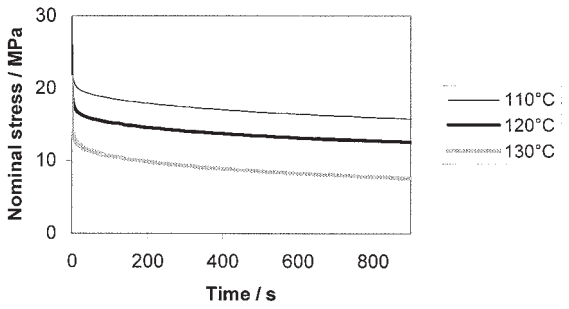

Figure 2 Constant-temperature stress relaxation at $\lambda = 2.08$.

controlled rate, during which time the specimen strain was kept constant or increased at a constant rate. To implement this last stage, we had to know the thermal deformation of the specimen and load train. This was then added to the desired mechanical deformation history, and the sum was programmed as the testing machine's displacement history.

To measure the thermal deformation for a particular experiment, we performed a separate experiment with the same temperature history while using the testing machine's load control to maintain effectively zero force. The machine motion was monitored and stored as a series of constant speed ramps. This enabled an appropriate series of speed ramps to be programmed for the stretching experiment.

As in the isothermal cases, both stress-relaxation and stress–strain experiments were performed. The stress relaxations were at extensions of 20 mm, and cooling was performed from 130 to 110°C at either 2.5×10^{-2} or 1.167×10^{-2}°C s^{-1}. In the stress–strain experiments, we used the same temperature regimen, with the extension increasing during cooling from 20 to 28 mm. The temperature field within the specimen was examined, as in the isothermal case, with a thermocouple embedded in the gauge length. During cooling, the air temperature and the internal specimen temperature differed by 0.8°C on average.

RESULTS AND MODELING: ISOTHERMAL CONDITIONS

Stress relaxation

The stress-relaxation results for the extension ratio of 2.08 are shown for 110, 120, and 130°C in Figure 2. The zero time was taken as the completion of the initial straining. The highest temperature experiment had a relatively long duration to supply necessary data for the anisothermal modeling (which is discussed later). The curves fit very well the Guiu–Pratt expression[21] derived from a model consisting of an Eyring process acting in series with an elastic element. The expression for the stress at time t [$\sigma(t)$] is given by

$$\sigma(t) = \sigma(0) - A\ln(1 + t/c) \quad (1)$$

where A and c are constants. On average, the experimental and modeled points differ by 1.4%. Equation (1) thus gives a useful representation of the curves and can be used for computational purposes.

A similar set of results for the extension ratio of 2.15 is shown in Figure 3. Equation (1) again gives a useful model, with an average error of 1.3%. The values of A and c are shown in Table I.

Stress–strain behavior

The results are shown in Figure 4 in the form of stress–extension curves at 130°C. After the stress drop accompanying the change to a lower rate at a 20-mm extension, the stresses rose, settling down to a constant rate of increase with the extension. The slopes for the linear parts of the curves do not differ systematically.

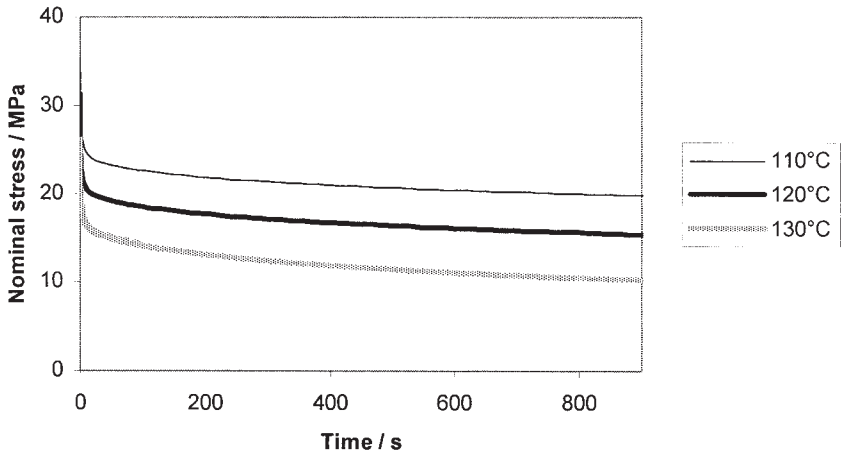

Figure 3 Constant-temperature stress relaxation at $\lambda = 2.15$.

TABLE I
Guiu–Pratt Parameters

	110°C			120°C			130°C		
λ	$\sigma(0)$(MPa)	A(MPa)	c(s)	$\sigma(0)$(MPa)	A(MPa)	c(s)	$\sigma(0)$(MPa)	A(MPa)	c(s)
2.08	62.1	2.07	9.74×10^{-4}	53.9	2.03	1.33×10^{-3}	44.2	2.35	6.45×10^{-3}
2.15	76.2	2.39	7.81×10^{-4}	67.3	2.47	8.71×10^{-4}	55.2	2.88	8.31×10^{-3}

Initial loading

In all the experiments, the specimen went through a stage of nonuniform deformation until the gauge was fully necked. The initial shear band evolved rapidly into an approximately symmetric neck. At the center of this neck, the strain conditions were essentially uniaxial, and the strains there were measured with image analysis. There were no detectable differences between the strain fields as the temperature varied in the range of 110–130°C. The strain rate as a function of the specimen extension was obtained by differentiation of the strain history and subsequent smoothing and is shown in Figure 5. The short time interval corresponding to shear banding, which was complete within the first 2 s (1.2-mm extension), was neglected. The maximum was characteristic of neck development, as was the extension at an essentially zero strain rate corresponding to steady-state neck propagation. After a 20-mm extension, the gauge length was fully necked, and the extension thereafter was at a constant strain rate.

Modeling

Here we present a unified model of the stress-relaxation and stress–strain behavior. The quality of the Guiu–Pratt fits to the stress-relaxation curves suggests the relevance of the Eyring process. The Guiu–Pratt model is of a linear elastic spring in series with an Eyring dashpot. For this purpose, the Eyring process can be represented by the equation linking the plastic strain rate ($\dot{e}_p$) to the stress (σ):

$$\dot{e}_p = \alpha \sinh(V\sigma) \tag{2}$$

α is a constant at a constant temperature, and V is related to the activation volume (v) by $V = v/kT$, where k is Boltzmann's constant and T is the absolute temperature. The spring of modulus E is strained by an amount e_e, and this results in a stress given by $\sigma = Ee_e$ and a total system strain given by $e = e_p + e_e$, where e_p is the plastic strain. Guiu and Pratt[21] assumed the argument $V\sigma$ to be large and replaced the hyperbolic sine function in eq. (2) with an exponential. For stress relaxation, when the total strain rate is $\dot{e} = 0$, the system can then be solved to give eq. (1). The constants in eq. (1) can be identified as follows:

$$A = \frac{1}{V} \tag{3}$$

$$c = \frac{1}{\alpha EV} \exp[-V\sigma(0)] \tag{4}$$

The results presented in Figure 4, in which the nominal stress (σ_n) increase linearly with extension, suggest the existence of an elastic mechanism when the material is stretched in its necked state. This follows from the experimental observation that, during slow stretching at extensions greater than 20 mm corresponding to the fully necked state, the strain rates are essentially constant, and at different testing speeds, the same strains are achieved at the same extension. The Gaussian model is the simplest theory that gives rise to the observed behavior at large defor-

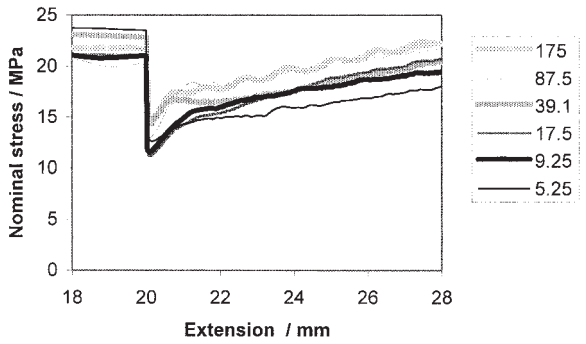

Figure 4 Experimental stress–extension curves. The inset lists the strain rates (10^{-6} s^{-1}) applied after 20 mm.

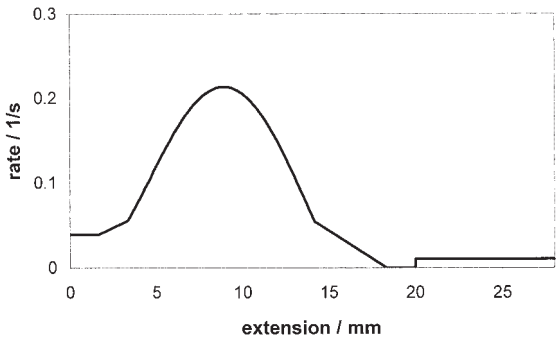

Figure 5 Strain rate history of the initial loading.

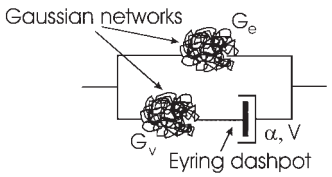

Figure 6 Constitutive model.

mations. In uniaxial extension with λ, the true stress (σ) is given by

$$\sigma = G(\lambda^2 - \lambda^{-1}) \tag{5}$$

This corresponds to σ_n (assuming incompressibility):

$$\sigma_n = G(\lambda - \lambda^{-2}) \tag{6}$$

where G is a material constant. For sufficiently large values of λ, the final term becomes negligible, and σ_n varies essentially linearly with λ.

These considerations lead us to construct a model, as illustrated in Figure 6. The upper arm consists of a Gaussian spring in series with an Eyring dashpot and gives both a Guiu–Pratt response under relaxation and rate-dependent yield behavior. This is in parallel with another Gaussian model, motivated by the elastic responses illustrated in Figure 4. For a constant applied rate of strain, the stress in the upper arm will reach a maximum level, depending on the strain rate, and then stay constant. Meanwhile, the stress in the lower arm will rise continuously to give a total σ_n value that rises as an essentially linear function of λ, as governed by eq. (6).

However, on examining the experimental data, we find that the quantitative application of the model is problematic. For the linear parts of the graphs in Figure 4, the slopes are on average given by $\partial\sigma_n/\partial\lambda$ = 67.4 MPa. Using the derivative of eq. (6) with a value of λ = 2.1, corresponding to the applied strain, then gives a value of $G \sim 61$ MPa. For the same strain, eq. (6) now gives a value of σ_n = 114 MPa, far in excess of the total observed σ_n value. σ_n is too low for the observed gradient, and so the extrapolated extension ratio corresponding to zero stress is around 2 rather than 0.

We have modeled this effect by assuming that the Gaussian network in the upper arm of the model only becomes operative when the material is in the fully necked state, corresponding to the extension ratio λ_0. The true stress for this elastic component (σ_e) is then given by the adaptation of eq. (5):

$$\sigma_e = \begin{cases} G_e\left[\left(\dfrac{\lambda}{\lambda_0}\right)^2 - \left(\dfrac{\lambda}{\lambda_0}\right)^{-1}\right] & \lambda > \lambda_0 \\ 0 & \lambda \le \lambda_0 \end{cases} \tag{7}$$

where G_e characterizes the upper network.

As we will show, the value λ_0 = 2.09 fits the observations well. Therefore, the stress-relaxation experiments at the lower extension ratio of 2.08 can be related to the parameters characterizing the network–dashpot pair in the upper arm of Figure 5. The stress in this viscoelastic system (σ_v) is related to the extension ratio in the upper Gaussian spring (λ_g) by

$$\sigma_v = G_v(\lambda_g^2 - \lambda_g^{-1}) \tag{8}$$

where G_v characterizes the lower network.

The same stress is also related to the strain rate in the Eyring process ($\dot{e}_p$) by the relation of eq. (2), which can be rewritten as follows:

$$\sigma_v = \frac{1}{V}\ln\left[\frac{\dot{e}_p}{\alpha} + \sqrt{\left(\frac{\dot{e}_p}{\alpha}\right)^2 + 1}\right] \tag{9}$$

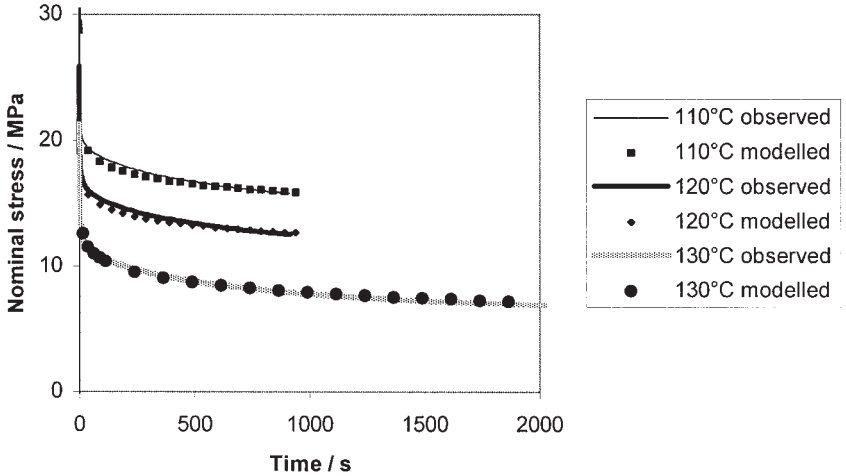

Figure 7 Modeling stress relaxation at λ = 2.08.

TABLE II
Model Parameters

	110°C	120°C	130°C
G_v (MPa)	2000	2000	2000
V (MPa^{-1})	0.46	0.49	0.42
α (s^{-1})	1.97×10^{-13}	1.53×10^{-12}	8.49×10^{-10}
G_e (MPa)	133	133	133
λ_0	2.09	2.09	2.09

For an extension ratio of the Eyring process (λ_p), the true strain rate is given by $\dot{e}_p = \dfrac{\dot{\lambda}_p}{\lambda_p}$. The extension ratios in the two mechanisms are related multiplicatively to the total extension ratio (λ)

$$\lambda = \lambda_g \lambda_p \tag{10}$$

with corresponding additive true strain rates.

The total stress (σ) is then given by

$$\sigma = \sigma_e + \sigma_v \tag{11}$$

The stress in the lower arm is calculated numerically. The time is increased incrementally, and the strains in the two elements are varied, under the constraint of eq. (11), to make σ_v, as calculated according to eqs. (8) and (9), sufficiently close, as defined by a predetermined convergence criterion. Equations (11) and (7) are then used to find the total stress.

Our first task is to model the stress-relaxation curves. The parameters for the Guiu–Pratt fits of Table I are related to the model parameters via eqs. (3) and (4), but it should be noted that eq. (1) is derived with the exponential approximation to the hyperbolic sine function, whereas our model uses the full function. The Table I values of A do, however, correspond quite closely to the values of V used in the model. The stress-relaxation curves do not provide sufficient information to provide separate values for all the model parameters, but eq. (4) (with $E = 3G_v$ at small strains) provides guidance for the trial-and-error process used to evaluate G_v and α. The model results have been calculated with a time increment of 0.25 s. Initial strain rate histories are as given in Figure 5. The parameters for modeling the stress relaxations at $\lambda = 2.08$ (G_v, V, and α) are included in Table II, and the modeled and observed results are shown in Figure 7. The fit is particularly good at 130°C and, typically of the other temperatures, is 1.2% on average at 110°C. The stress relaxations at $\lambda = 2.15$ are modeled with the same parameters, but at this higher strain the parallel network characterized by G_e contributes to the stress. Thus, according to the model, at a given temperature, the stress at the higher strain exceeds the stress at the lower strain by a constant. The observed and modeled curves at the higher strain are shown in Figure 8. The prediction errors are similar at 110 and 130°C, being typically around 8%. The value of G_e is that obtained from the fitting to the stress–strain curves, as discussed next.

For the stress–strain experiments, the strain rate history, used as input for the model, consists of that of Figure 5, up to 20-mm extension, followed by the appropriate constant rate. The value of G_e is obtained by the matching of the slopes of the linear parts of the σ_n–extension predictions with the average of the corresponding slopes in the graphs shown in Figure 4. Figure 9 shows the model predictions to be compared with Figure 4. The predicted curves are simpler than the observations because they lack the initially high slopes occurring as the stress increases after 20-mm

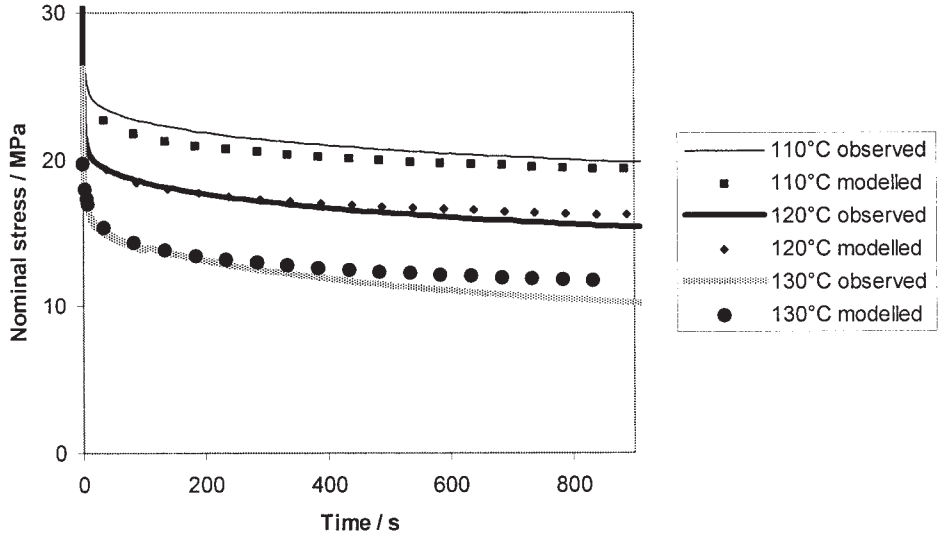

Figure 8 Modeling stress relaxation at $\lambda = 2.15$.

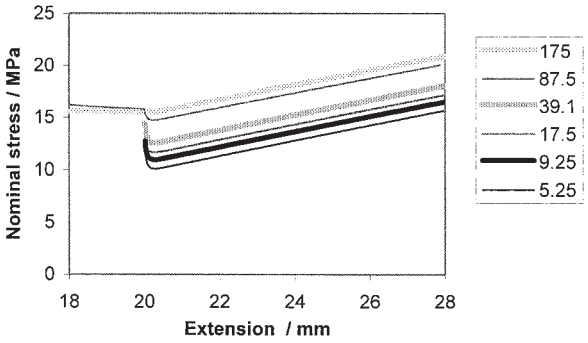

Figure 9 Model stress–extension curves. The inset lists the strain rates (10^{-6} s^{-1}) applied after a 20-mm extension.

extension. Therefore, as a result of G_e being chosen to give the correct slopes, the predictions of the values are low (by 12% on average for the stress values at 28-mm extension).

Although the values of the parameters have been obtained with reference to stress relaxation and slow stress–strain experiments, it is interesting to examine how the model, as presently constituted, responds to the fast strain inputs associated with the initial loading. The strain rate history of Figure 5 is used in the model at the three temperatures, and the stress predictions are compared with observations in Figure 10. The predicted stresses are of the correct order and show characteristic peaks typical of the Eyring yield event. The model stresses are not accurate in detail, as they are based on strain rate histories that are themselves not known in detail, given the 2-s image capture interval.

We would not expect a model as simple as that proposed here to represent well all details of the material behavior. The quality of the modeling, as illustrated in Figures 7–10, suggests, however, that it may be a useful tool. We shall show in the following sections that it can be generalized usefully to explore the principles governing anisothermal material behavior.

RESULTS AND MODELING: ANISOTHERMAL CONDITIONS

Stress relaxation

Before applying the theory developed so far, we examine a simple relationship between isothermal and anisothermal stress relaxation. We postulate that, for stress relaxation in which the temperature changes continuously, the rate of stress decay is the same as that which would apply under isothermal conditions for the same temperature, strain, and time after loading. At a given strain, with the stress in relaxation at a constant temperature $T(t)$ at time t after loading denoted by $\sigma_i(t,T)$, the stress in the anisothermal stress relaxation at the same strain (σ_a) is then given by

$$\sigma_a[t,T(t)] = \sigma_i[0,T(0)] + \int_0^t \frac{\partial \sigma_i[\tau,T(\tau)]}{\partial \tau}\, d\tau \qquad (12)$$

where τ is the instantaneous time and the strain has been applied at zero. For convenience, we have used eq. (1) to approximate the stress-relaxation curves when implementing this model. The integrand in eq. (12) is then simply $\{A[T(\tau)]\}/\{c[T(\tau)] + \tau\}$. The results have been calculated for stress relaxation at the extension ratio of 2.08 as the specimen cools from 130 to 110°C. The integrals have been calculated numerically (numerical algorithms group subroutine D01AHF), with the values of A and c given in Table I, with values at intermediate temperatures derived with linear interpolation. The predictions are compared with the observations in Figure 11(a,b) for the cooling rates of 2.5×10^{-2} and 1.167×10^{-2}°C s^{-1}. The observed and model curves are acceptably close. Over the temperature range considered, the rate of stress decay does not

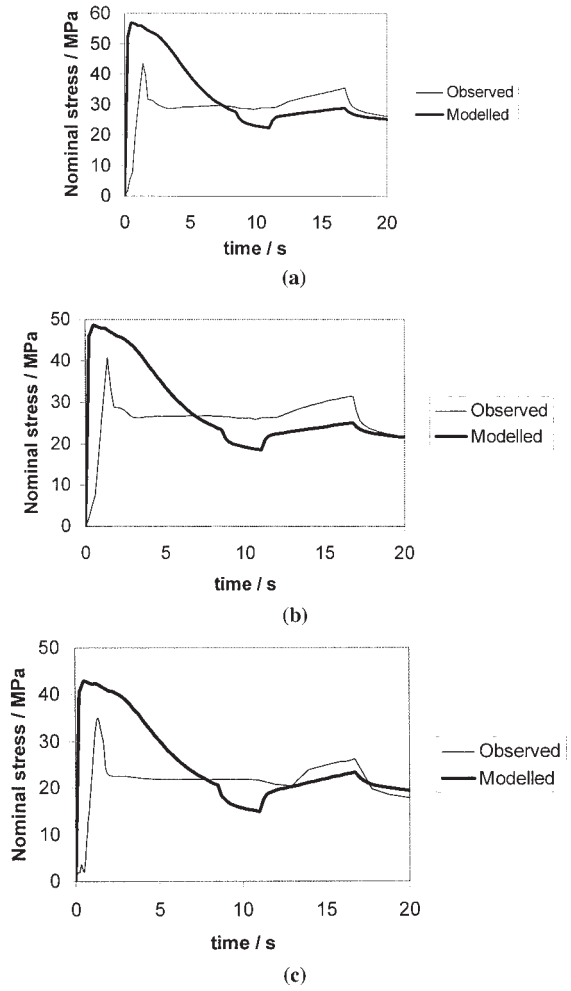

Figure 10 Initial material response at (a) 110, (b) 120, and (c) 130°C.

vary greatly as a function of temperature, and so there is no scope for exploring the applicability of time–temperature superposition: stress-relaxation curves at different temperatures essentially differ by a constant.

The model of Figure 6 has been generalized to anisothermal conditions by the introduction of temperature dependence into the parameters of Table II. V and α are assumed to depend only on the current temperature. Experiments similar to those of Figure 4 but at lower temperatures have not revealed any significant change in G_e; the material certainly becomes stiffer upon cooling, but this is modeled by the temperature dependence of the lower arm of the model in Figure 6. The same stress-relaxation experiments described previously, at an extension ratio of 2.08 for the two cooling rates, were modeled by the application of a strain rate history, as defined in Figure 5, for the first 12 s, followed by a zero strain rate. The values of V and α for temperatures lying between the measurement temperatures were obtained by interpolation. Linear interpolation is adequate for V but is clearly unjustifiable for α, which varies much more between 120 and 130°C than between 110 and 120°C. The values used in the calculations were obtained by linear least-squares fitting of the logarithm of α. The results are compared with observations in Figure 12(a,b) for the cooling rates of 2.5×10^{-2} and 1.167×10^{-2}°C s^{-1}. The fits to the observations are clearly less good than

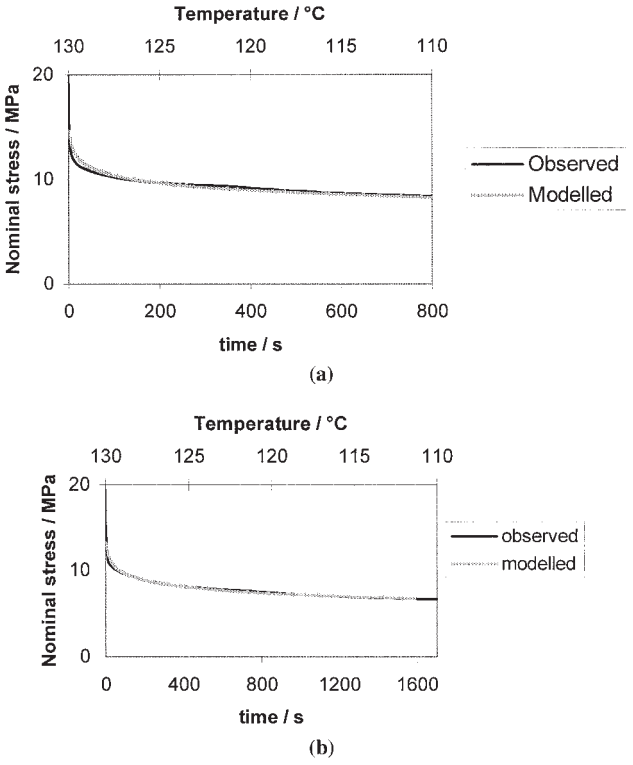

Figure 11 Stress relaxation modeled with eq. (12) for cooling at (a) 2.5×10^{-2} and (b) 1.167×10^{-2}°C s^{-1}.

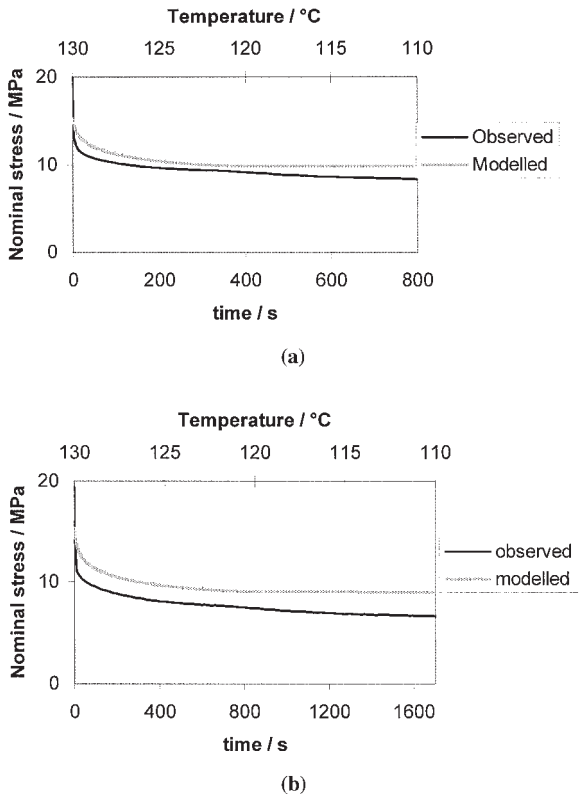

Figure 12 Stress relaxation modeled with the model of Figure 6 for cooling at 2.5×10^{-2} °Cs^{-1}. Average prediction error 11%. (b) Stress relaxation modelled using model of Figure 6 for cooling at 1.167×10^{-2} °Cs^{-1}

those of Figure 11, in which the anisothermal stress relaxation is derived from the isothermal stress relaxation.

Stress–strain behavior

Three cooling rates have been applied: the same two used for stress relaxation and the slowest rate available from the control system. Constant rates for both the temperature change and strain were applied, with the temperature falling from 130 to 110°C while the extension ratio was increased from 2.08 to 2.15. The strain rates ($d\lambda/dt$) were 4.08×10^{-5}, 8.75×10^{-5} s^{-1}, and 5.86×10^{-6} s^{-1}, corresponding to cooling rates of 1.167×10^{-2}, 2.5×10^{-2}°C s^{-1}, and 1.67×10^{-3}°C s^{-1}, respectively. The model parameters and interpolation methods were the same as those used for stress relaxation. The results are shown in Figure 13. The predicted stresses are significantly lower than the observations, and this shows a similar quality of prediction at all rates.

DISCUSSION

Under isothermal conditions, there is consistency between the Guiu–Pratt fitting of the stress-relaxation

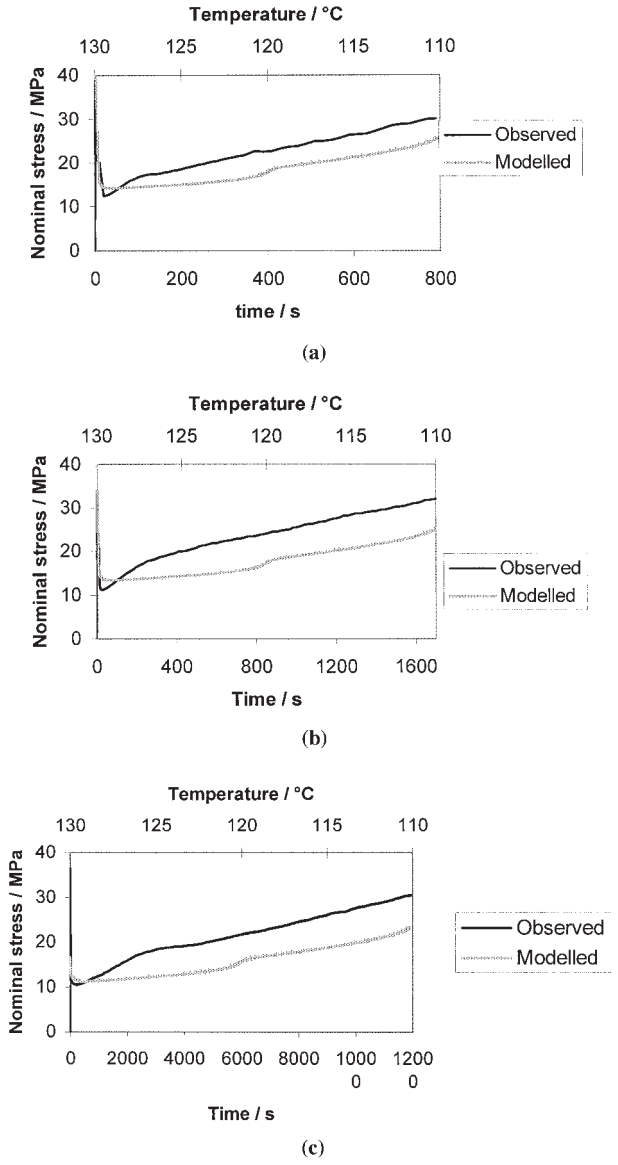

Figure 13 Stress–strain behavior (a) for stretching at a strain rate of 8.75×10^{-5} s^{-1}, modeled with the model of Figure 6 for cooling at 2.5×10^{-2} °Cs^{-1}. (b) Stress-stain behaviour for stretching at a strain rate 4.08×10^{-5} s^{-1}, modelled using the model of Figure 6 for cooling at 1.167×10^{-2} °Cs^{-1}. (c) Stress-strain behaviour for stretching at a strain rate 5.86 x 10^{-6} s^{-1}, modelled using the model of Figure 6 for cooling at 1.67×10^{-3} °Cs^{-1}.

curves and the Eyring parameters in the constitutive model. The constitutive model generally performs well. Its most unusual feature is the parallel Gaussian network characterized by G_e, which only becomes active just beyond the material's natural draw ratio. We are led to the inclusion of this mechanism by (1) the linear increase in σ_n with the extension ratio upon the stretching of the necked material, which is highly suggestive of a Gaussian network, and (2) the gradient of this stress increase being such that, upon extrapolation back to zero stress, the corresponding strain value is finite.

The work of Zhou et al.[9] is relevant to the discussion of the physical origin of this component. They postulated that, upon yielding, polycarbonate undergoes a transition into a rubbery state and returns to the glassy state upon unloading. The temperature measurements of the developing neck support this concept, a stress-induced mesostate. Also of relevance is the interpretation of Nanzai[13] and Nanzai et al.[22] that solid polycarbonate is transformed into meltlike structures during yielding. If our specimens indeed enter such a rubber state upon yielding, the question arises of the state of the postyield necked material at and beyond the natural draw ratio. We have explored the state of matter represented by the parallel network in our model by investigating the number of crosslinks (N) that correspond to the parameter G_e, given by $G_e = Nk_BT$, where k_B is Boltzmann's constant. The value of N is thus found to correspond to approximately eight links per repeat unit. Clearly, this does not relate to the physics of a freely jointed molecular chain, and any physical justification for the use of the Gaussian theory disappears (although we retain the numerical formulation as an appropriate representation of the linear process). Moreover, this finding implies a degree of constraint incompatible with the rubbery state.

This suggests that, after yielding and necking, the material reverts to a glassy state. The formation of the glassy state was considered by Edwards and Vilgis,[23] who envisaged that, as rubber transforms into glass, molecular chains become increasingly constrained at pinch points along their lengths. This leads to the expectation that new constraints will form in the polycarbonate after necking, which we can associate with the linear component characterized by G_e and becoming active at λ_0. Recently, Stachurski[24] further explored the concept of the evolution of constraints associated with the glass transition by computer simulation with Voronoi tessellation. Molecular chains pass through constriction points associated with locally high density, at which the chain mobility is highly limited (and far from freely jointed). Plastic behavior is associated with the tension in the chain becoming large enough for it to be pulled through the constriction point.[23,25] These ideas lead us to propose that the observed linear component arises from a network of constriction points that form upon reversion to the glassy state. Further theoretical work is required to determine whether our observed value of G_e is consistent with this picture.

The parameter V in Table II corresponds, on average, to $v = 2.5$ nm^3. This is comparable with the value of 6.4 nm^3 recorded by Haward and Thackray.[18] Bauwens-Crowet et al.[26] reported experimental data equivalent to a value of 3.4 nm^3. Spathis and Kontou[12] deduced from measurements of polycarbonate separate pressure and shear activation volumes (v_p and v_s, respectively). For our uniaxial tensile tests, v as de-

fined in our model is equal to $\frac{1}{3}v_p + v_s$, for which their data give a figure of 1.7 nm^3. These examples show a degree of consistency between our values and those of other workers.

For the prediction of anisothermal stress relaxation, eq. (12) proves more effective than the constitutive model. The process of using eq. (12) involves the fitting of relaxation curves to eq. (1). The values of the parameters A and c thus derived vary far less with temperature than the parameter α in the constitutive model, and so interpolation for values at intermediate temperatures poses less of a problem. The different quality of the prediction may, therefore, in part reflect numerical effects. However, the two models are essentially different. If we assume (as is the case for $\lambda = 2.08$) that the stress in the constitutive model is that in the series model that constitutes the lower arm of Figure 6, then we can arrive at an expression for the rate of stress decay. For λ_p, we can approximate eq. (9) for a large argument by

$$\sigma = \frac{1}{V} \ln\left(\frac{2\dot{\lambda}_p}{\alpha\lambda_p}\right) \tag{13}$$

to give the total stress (σ). σ is also equal to that in the series network, which can be approximated for large λ_g values by

$$\sigma = G_v\lambda_g^2 \tag{14}$$

It now becomes possible to use eq. (10) in eq. (14) and thence to derive expressions for λ_p and $\dot{\lambda}_p$ in terms of σ and $\dot{\sigma}$. The substitution and rearrangement of eq. (13) then give an expression for the decay rate of stress:

$$\dot{\sigma} = -\frac{\alpha\sigma\exp(V\sigma)}{\lambda G_v} \tag{15}$$

From this, it is clear that, as the stress increases, the absolute value of its rate of decay does as well. As in most viscoelastic systems, including linear viscoelasticity, stress relaxation is driven by the level of stress. This in contrast to eq. (12), which is based on the premise that the rate of relaxation of stress depends only on the temperature and the time after loading. Now consider a specimen in stress relaxation that has cooled to a temperature T. The stress will be lower than that for a specimen that has been relaxing for the same time at a constant temperature T. Therefore, according to eq. (15), the rate of stress decay will be lower for the cooling specimen, whereas according to eq. (12), the decay rates will be the same. Therefore, our constitutive model of Figure 6 will predict higher stresses than eq. (12). A comparison of the numerical results in Figures 11 and 12 shows that they conform to this expectation. A model based on the Eyring process could be constructed to have the same temperature/stress-relaxation characteristic as eq. (12) if we could ensure that only a (temperature-dependent) fraction of the total stress was relaxing. This could be done by the addition of a permanent elastic, or more slowly relaxing, process in parallel to the model in Figure 6. Such a model would make improved predictions of stress relaxation, but the added parallel process would need to be highly temperature-dependent, and this would lead to more complex behavior for anisothermal stretching. If the added process were elastic, it would need to increase in stiffness during cooling, and this would result in a stress–strain curve with increasing slope, in contrast to the observations in Figure 13. A more complex model along these lines might be worthy of future study.

In contrast to stress relaxation, the anisothermal stress–strain behavior, as shown in Figure 13, is underpredicted by the constitutive model. It is significant that the stress relaxations are at the extension ratio of 2.08, and so the model does not include the effects of the parallel elastic network parameter G_e, whereas the stress–strain curves are at a higher strain. The characteristic of underprediction is also apparent in the modeling of isothermal stress–strain curves, as shown in Figures 4 and 9, but not in the modeling of isothermal stress relaxation, as shown in Figure 8. Thus, there is a level of consistency between the isothermal and anisothermal performances of the model.

CONCLUSIONS

We have produced experimental data on the tensile stress–strain behavior of necked and necking polycarbonate at elevated temperatures below the glass transition, under both constant and falling temperature conditions. A nonlinear constitutive model has been developed that incorporates an Eyring process and an elastic network, with the latter becoming effective only in the postnecking regimen. We have adopted the concept, introduced by previous workers, of a glass–rubber–glass transition as a possible mechanism for the origin of this delayed elastic component. Stress-relaxation and stress–strain experiments have been used to verify the model. Anisothermal experiments are predicted with less accuracy than isothermal ones, but the accuracy is still at a useful level. In addition, an empirical integral relation has been shown to be capable of deriving anisothermal stress-relaxation curves from isothermal curves.

References

1. Caton-Rose, P.; Sweeney, J.; Collins, T. L. D.; Coates, P. D. Plast Rubber Compos 2000, 29, 51.
2. Lai, J. S. Y.; Findley, W. N. Trans Soc Rheol 1973, 17, 63.

3. Buckley, C. P. Rheol Acta 1988, 27, 224.
4. Drozdov, A. D. Polym Eng Sci 1997, 37, 1983.
5. Nied, H. F.; Stokes, V. K.; Ysseldyke, D. A. Polym Eng Sci 1987, 27, 101.
6. Nazarenko, S.; Bensason, S.; Hiltner, A.; Baer, E. Polymer 1994, 35, 3883.
7. Boyce, M. C.; Arruda, E. M. Polym Eng Sci 1990, 30, 1288.
8. Boyce, M. C.; Arruda, E. M.; Jayachandran, R. Polym Eng Sci 1994, 34, 716.
9. Zhou, Z.; Chudnovsky, A.; Bosnyak, C. P.; Sehanobish, K. Polym Eng Sci 1995, 35, 304.
10. Masud, A.; Chudnovsky, A. Int J Plast 1999, 15, 1139.
11. Bauwens-Crowet, C.; Bauwens, J. C.; Homès, G. J Polym Sci Part A-2: Polym Phys 1969, 7, 735.
12. Spathis, G.; Kontou, E. Polym Eng Sci 2001, 41, 1337.
13. Nanzai, Y. J Non-Cryst Solids 1991, 131, 516.
14. Halsey, G.; White, H. J.; Eyring, H. Text Res J 1945, 15, 295.
15. Argon, A. S. Philos Mag 1973, 28, 839.
16. Boyce, M. C.; Parks, D. M.; Argon, A. S. Int J Plast 1989, 5, 593.
17. Wu, P. D.; van der Giessen, E. J Mech Phys Solids 1883, 41, 427.
18. Haward, R. N.; Thackray, G. Proc R Soc London Ser A 1968, 302, 453.
19. Lundberg, L.; Jansson, J.-F. Polymer 1994, 35, 2084.
20. Haynes, A. R.; Coates, P. D. J Mater Sci 1996, 31, 1843.
21. Guiu, F.; Pratt, P. L. Phys Status Solidi 1964, 6, 111.
22. Nanzai, Y.; Yamasaki, T.; Yoshioka, S. JSME Int J Ser A 1998, 41, 31.
23. Edwards, S. F.; Vilgis, T. Polymer 1987, 28, 375.
24. Stachurski, Z. H. Polymer 2003, 44, 6059.
25. Stachurski, Z. H. Polymer 2003, 44, 6067.
26. Bauwens-Crowet, C.; Bauwens, J. C.; Homès, G. J Polym Sci Part A-2: Polym Phys 1969, 7, 1745.